Phase I Technical Report.

Phase I grant award Number: DE-SC0011330

Company: Electron Optica, Inc.

Title: Mirror monochromator

Topic: 5 - Instrumentation for Electron Microscopy and Scanning Probe Microscopy

Subtopic: a - Electron Microscopy and Spectroscopy

Principal Investigator: Marian Mankos

Rights in Data – SBIR/STTR Program.

Note: This report does not include any proprietary data.

Summary.

In this SBIR project, Electron Optica, Inc. (EOI) is developing a mirror electron monochromator (MirrorChrom) attachment to new and retrofitted electron microscopes (EMs) for improving the energy resolution of the EM from the characteristic range of 0.2-0.5 eV to the range of 10-50 meV. This improvement will enhance the characterization of materials by imaging and spectroscopy. In particular, the monochromator will refine the energy spectra characterizing materials, as obtained from transmission EMs [TEMs] fitted with electron spectrometers, and it will increase the spatial resolution of the images of materials taken with scanning EMs (SEMs) operated at low voltages.

EOI's MirrorChrom technology utilizes a magnetic prism to simultaneously deflect the electron beam off the axis of the microscope column by 90° and disperse the electrons in proportional to their energies into a module with an electron mirror and a knife-edge. The knife-edge cuts off the tails of the energy distribution to reduce the energy spread of the electrons that are reflected, and subsequently deflected, back into the microscope column. The knife-edge is less prone to contamination, and thereby charging, than the conventional slits used in existing monochromators, which improves the reliability and stability of the module. The overall design of the MirrorChrom exploits the symmetry inherent in reversing the electron trajectory in order to maintain the beam brightness – a parameter that impacts how well the electron beam can be focused downstream onto a sample.

During phase I, EOI drafted a set of candidate monochromator architectures and evaluated the trade-offs between energy resolution and beam current to achieve the optimum design for three particular applications with market potential: increasing the spatial resolution of low voltage SEMs, increasing the energy resolution of low voltage TEMs (beam energy of 5-20 keV), and increasing the energy resolution of conventional TEMs (beam energy of 80-120 keV).

Specialized software packages that have been developed by MEBS, Ltd. were used to calculate the electron optical properties of the key monochromator components: namely, the magnetic prism, the electron mirror, and the electron lenses. In the final step, these results were folded into a model describing the key electron-optical parameters of the complete monochromator. The simulations reveal that the mirror monochromator can reduce the energy spread of a Schottky electron source, an established electron emitter used widely in EMs, to 10 meV for practical beam current values and that further reduction of the energy spread down to 3 meV is possible for low current applications with a Cold Field Emitter (an electron source with 10x the brightness of a Schottky source).

MirrorChroms can be designed and built to attach to different types of TEMs and SEMs, thus making them suitable for enhancing the study of the structure, composition, and bonding states of new materials at the nanoscale to advance material science research in the field of nanotechnology as well as biomedical research.

I. Phase I Technical Objectives.

The goal of this project is to establish the feasibility of a monochromator that is capable of reducing the energy spread of electron sources used in transmission (TEM) and scanning (SEM) electron microscopes to values in the range of 10-50 meV in general and to values less than 10 meV for specific applications. The key insight of Electron Optica's mirror monochromator approach is the exploitation of mirror symmetry, which allows the use of a knife-edge aperture as the energy-selecting device. This approach has two major advantages compared to existing monochromator designs: first, narrow, sub-micron slits are not required, and second, the energy resolution is determined by the optics, rather than the aperture (slit) width.

Technical Approach

Electron Optica proposes to develop a novel monochromator that reduces the energy spread of commonly used electron sources into the 10-50 meV range. The design of the monochromator accommodates existing electron sources and is suitable for both TEMs and SEMs.

The monochromator design utilizes an electrostatic electron mirror combined with an energy-dispersive beam separator and a knife-edge aperture [Mankos[a]] to filter electrons with energies that are lower or higher than the selected nominal energy, E_0. Electrons emitted by the source are deflected by the beam separator off the beam axis towards the electron mirror, as shown in Fig. 1. The beam separator, a magnetic prism array, deflects the electrons with nominal beam energy E_0 (green line) by 90 degrees, while electrons with a slightly lower (red line) or higher energy (purple line) are deflected slightly more or less, respectively, as a result of the energy dispersion of the beam separator. As the electrons proceed towards the mirror, the knife edge aperture stops the lower energy tail of the energy distribution. After reflection in the mirror, the higher energy tail is stopped on the same knife edge. Consequently, the width of the energy spread of the electron beam that passes can be selected simply by moving the knife edge aperture in or out of the beam path. The fraction of the beam that returns back into the column is then characterized by a lower energy spread. The use of a knife edge as the energy selecting device is key: it makes for a more reliable aperture when compared to the narrow, often sub-micrometer slits needed in existing monochromators. Here, it is the optics, rather than the slit width, that sets the ultimate energy resolution. After the double pass through the monochromator, the energy dispersion introduced by the beam separator vanishes due to the symmetry in the design. If the net dispersion of the monochromator were not to vanish, the resulting spread in the beam would introduce additional aberrations that would degrade the resolution.

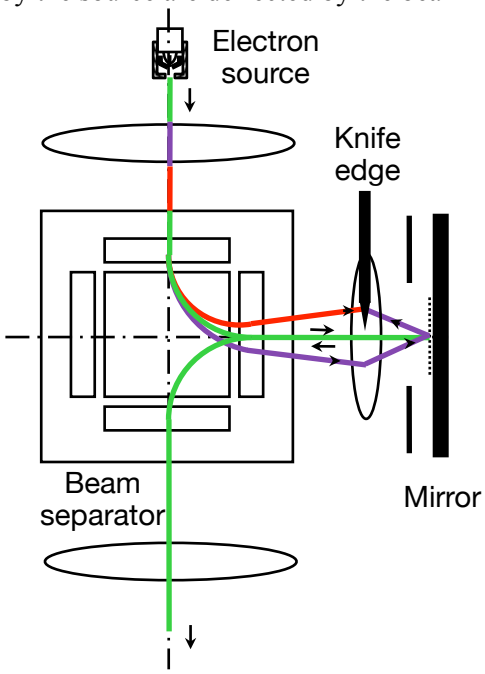

Figure 1. Monochromator principle.

In order to establish the feasibility of this novel instrumentation, Electron Optica focused the phase I research on six key objectives:

1. Review candidate architectures

Evaluate possible layouts including a variety of electron sources, beam separators, electron mirrors and electron lenses by analyzing 1st order optics of the monochromator design options. Select the most promising candidate for TEM (20-100 keV) and SEM (1-20 keV).

2. Establish the optical properties of the magnetic beam separator

Analyze the optical properties of the magnetic beam separator by modeling its focusing properties, energy

dispersion, and aberrations. Show that an energy resolution of 10 meV or less is achievable in a practical separator geometry.

3. Establish the optical properties of the electron mirror

Analyze the optical properties of the electrostatic electron mirror by modeling its focal length, imaging properties, and aberrations up to 3rd order. Demonstrate that the electron mirror aberrations do not significantly degrade the energy resolution.

4. Minimize the aberrations of the electron-optical lenses

Evaluate the contribution of the gun and transfer electron lenses by analyzing their optical aberrations up to 3rd order. Demonstrate that the lens aberrations do not significantly degrade the energy resolution.

5. Determine the impact of Coulomb interactions

Analyze the energy resolution as a function of beam current and beam energy by incorporating the effect of Coulomb interactions with the optical aberrations. Determine the range of beam currents and energies where the impact of Coulomb interactions does not significantly degrade the energy resolution.

6. Establish the electron-optical parameters of the complete system

Determine the energy resolution and the aberrations of the complete monochromator system including the electron source, the beam separator, the electron mirror, and the lenses. Derive the electron-optical parameters for the complete monochromator.

II. Phase I Accomplishments.

The following section describes the results and activities performed during phase I that were required to remove the technical risks and validate the novel concepts described in the previous section. The results are grouped into six tasks, matched to the six technical objectives discussed in the previous section.

Task 1. Study candidate architectures.

The main electron-optical components of the monochromator, the electron source, the beam separator, the electron mirror, and the illumination, transfer and projection electron lenses are shown in Fig. 2. Electron sources most commonly used in TEMs and SEMs are thermionic emitters (W, LaB_6) and thermally assisted (Schottky) field emitters, which produce an electron beam with an energy spread in the range of 0.5 eV to 2 eV. Cold field emitters (CFEs), on the other hand, have the lowest energy spread, approaching 0.2 eV. The monochromation of these sources depends in part on their brightness, which varies over three orders of magnitude as shown in Table 1.

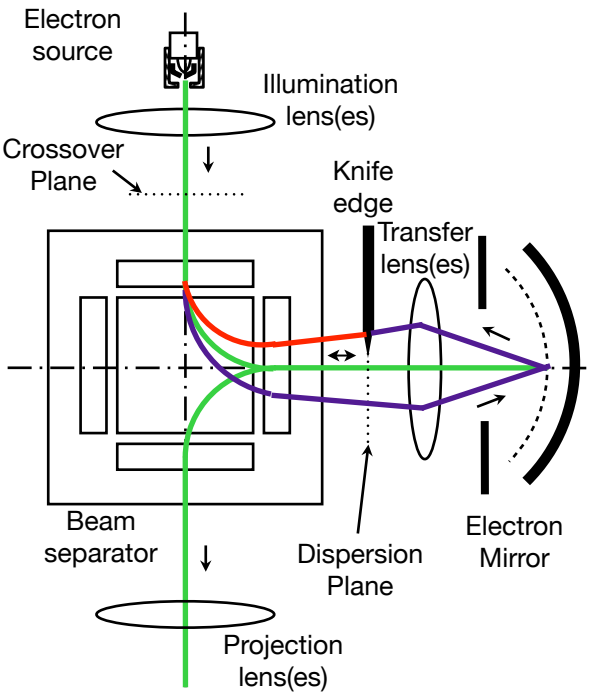

Figure 2. Key monochromator components.

The beam separator is based on a magnetic prism array, a proven and reliable design, which has been developed for low energy electron microscopes (LEEMs) to separate the otherwise overlapping illumination and projection optics [Mankos[b]]. The array of lenses in the prism maps a given object plane upstream from the prism with unit magnification onto the corresponding image plane while simultaneously dispersing the beam according to the electron energies. A typical separator geometry with an overall dimension of 100 mm x 100 mm disperses a beam of electrons

Electron Emitter	Red. brightness B' [A / (m^2·sr·V)]	Source size S [nm]	Energy spread ΔE [eV]
LaB_6	$2 \cdot 10^5$	20,000	0.5 - 2
Schottky	$2 \cdot 10^7$	25	0.5
CFE	$2 \cdot 10^8$	10	0.2

Table 1. Electron source parameters.

with a nominal energy of 5 keV by 10 μm/eV. The energy dispersion increases approximately linearly with the size of the separator and is inversely proportional to the beam energy. Consequently, it can be expressed as

$$D\ [\mu m/eV] \cong 500\ L\ [m] / E\ [keV]$$

To monochromate the beam, the illumination optics is tuned to form a beam crossover (a magnified image of the virtual source) upstream from the prism at a plane that is conjugate to that of the knife-edge. The size of the beam crossover will, in general, not only have contributions from the virtual source size, it will also have contributions from diffraction at the aperture and from the aberrations of the transfer lenses in the illumination optics. As will be shown in a following section, the aberrations from the transfer lenses may be neglected, leaving only the first two contributions. According to *Kruit* [Kruit], the magnified virtual source size, S_I, and the diffraction spot from the Airy disc, S_A, add approximately as

$$S_{50}^n \cong S_I^n + S_A^n : n = 1.3$$

where S_{50} is the spot diameter containing 50% of the current. If the current density were to be approximated as a two-dimensional Gaussian with a standard deviation of σ, then S_{50} would correspond to the full-width at half max (FWHM) of the distribution or 2.35σ. The magnified source size is derived from the spot area

$$\mathrm{A} = \frac{\pi}{4} S_I^2$$

which gives the beam current I that can be packed into the spot as

$$I = B' \cdot A \cdot \Omega \cdot E$$

where B' is the source brightness reduced by the beam energy (a conserved quantity) and Ω is approximately the solid angle captured by the beam convergence angle at the crossover α,

$$\Omega = \pi\, \alpha^2$$

The diffraction spot is derived from the de Broglie wavelength λ as

$S_A \cong 0.54\ \lambda / \alpha$

$\lambda\ [nm] = 1.226/\sqrt{(E[V])}$

The prism images this spot onto the plane of the knife-edge with unit magnification. The spot size here determines the energy resolution of the monochromator. If the aberrations in the prism could be ignored, then the spot size at the knife-edge would equal S_{50}. However, the prism aberrations cannot be made arbitrary small owing to the $1/\alpha$ scaling of S_{50}. Hence, the convergence angle must be optimized in order to minimize the spot size S resulting from the convolution of S_{50} with the prism aberrations. As discussed in the next section, the optimized convergence angle is found to be in the range of $0.1\ mrad < \alpha \leq 1\ mrad$. To deliver the required convergence angle and crossover position for a range of operating modes, more than one lens may be needed in the illumination optics.

Ideally, the transmission of the electrons at the knife-edge would be unity for those with energies inside the window and zero outside. In practice, however, a finite S smears the boundary of this window, degrading the transmission function. To minimize the impact of the tapered boundary, a lower limit must be set on the energy window and thereby on the degree to which the beam can be monochromated. The lower limit is set as the ratio of S to the dispersion in the separator; that is,

$$\delta E\ [eV] \cong S\ [\mu m] / D\ [\mu m/eV]$$

This ratio gives the minimum energy difference between two groups of electrons whose spots can be clearly separated at the knife-edge. For example, an energy dispersion of 10 µm/eV can separate two spots of size 0.1 µm formed by two groups of electrons with an energy difference of 10 meV.

The monochromator will reduce this current by removing the electrons with energies that fall outside the window δE about the nominal beam energy. The fraction of the electrons that pass through this window is a function of the source energy distribution F. Using experimental data on a Schottky electron source, a model, universal curve for this distribution has been derived as

$$\ln F(u) = c + \begin{Bmatrix} -\frac{1}{2}(ku)^2 : |ku| \leq 1 \\ -|ku| + \frac{1}{2} : |ku| > 1 \end{Bmatrix}$$

where c is a normalization constant, $k = \sqrt{(8 \ln 2)}$, and u is the difference in the electron energy from the nominal beam energy E_0 divided by the source energy spread ΔE, which is measured as the full-width at half-max of the distribution. The data and the universal curve are shown in Fig 3a. Here, the asymmetry in the experimental data about $u = 0$ has been ignored as it does not influence the results for the practical case where the energy window samples the center of the distribution.

The fraction of electrons that are transmitted, T, is derived from a convolution of the energy distribution with the transmission function of the window, which is approximated as a rectangular function with width $\delta E/\Delta E$. The transmitted fraction is plotted as a function of the width of the energy window and its center offset in Fig. 3b. The window width and offset are normalized to ΔE so that the graph may also be applied as a model for the other sources. As evident in Fig. 3b, the deviation in the tail of the experimental data from an exponential drop with u as modeled by $F(u)$ does not materially impact the transmitted fraction. Practical values for the misalignment in the window position, equivalent to 10% of ΔE, also have a negligible impact on the transmission. For the case in practice, where $\delta E \ll \Delta E$, the transmitted fraction can be approximated as

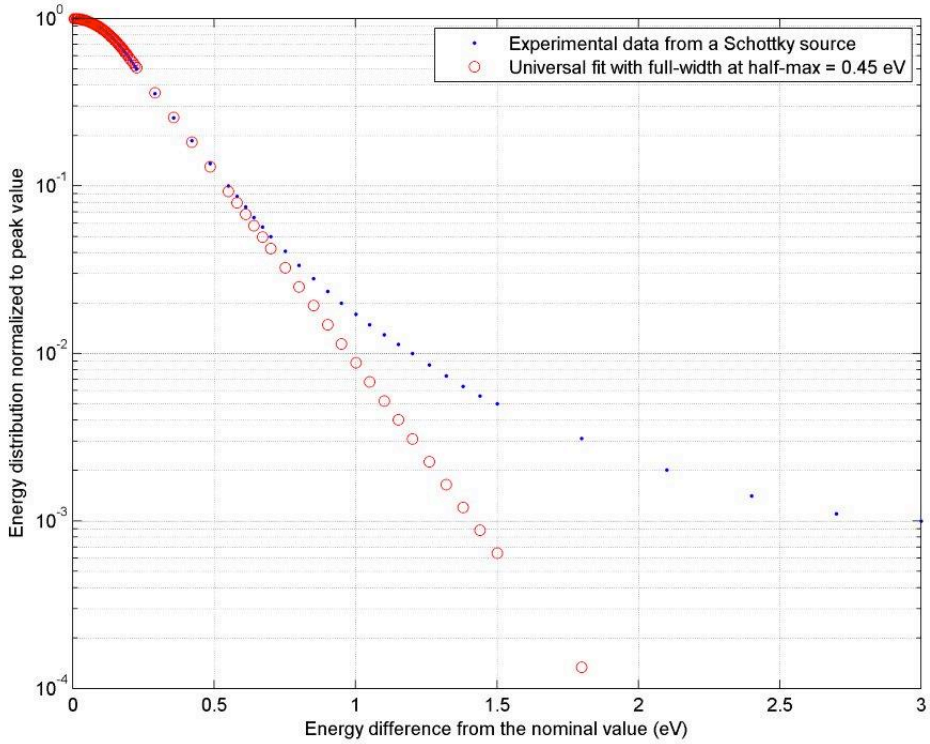

Figure 3a. Electron energy distribution.

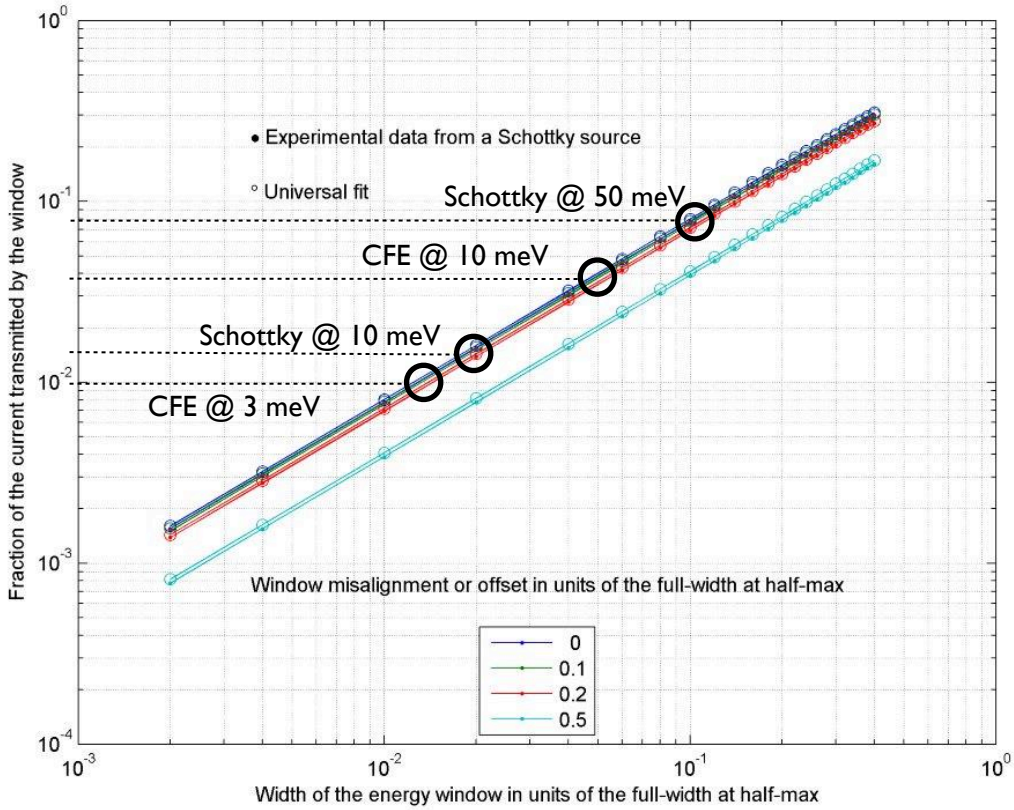

Figure 3b. Fraction of transmitted current vs. energy window.

$$T \cong 0.8\, \delta E / \Delta E$$

Hence, an energy window of δE =10 meV will transmit about 1.5% of the current from a Schottky emitter (ΔE = 0.5 *eV*) and about 4% of the current from a CFE (ΔE = 0.2 *eV*).

By neglecting the contributions of diffraction and of the prism aberrations to the spot size at the knife-edge, an upper bound is derived for the transmitted current *I'*, after monochromation, as a function of the reduced brightness *B'*, the source energy spread ΔE, the beam energy *E*, the beam convergence angle at the crossover α, the size of the beam separator *L*, and the energy window of the monochromator δE as

$$I'[nA] \cong 5 \cdot 10^{-1} (\alpha[mrad])^2 \frac{B'[A/(m^2 srV)]}{\Delta E[eV]} \cdot \frac{L^2[m^2]}{U[keV]} \cdot (\delta E[eV])^3$$

If the source energy spread is monochromated to a value of 10 meV with the aforementioned beam separator (*L* = 0.1 m), the upper bound on the current that could be transmitted to the sample by a 5 keV beam that originates from a CFE source is about 1 nA. This current would drop by a factor of 25 to 40 pA for a Schottky emitter. The LaB_6 emitter would deliver a meager 0.1 pA to the sample, making its use impractical.

The transmitted current scales with the cube of the energy window, $I' \propto (\delta E)^3$, highlighting a sensitivity to the energy resolution. This sensitivity bifurcates the application space for the monochromator to high speed imaging applications that work with a moderate energy resolution and to high-end spectroscopic applications that sacrifice sample current for energy resolution. Furthermore, the scaling of *I'* with the separator dimension and beam energy, $I' \propto L^2 / E$, lends itself to a compact design for the lower energy, imaging and spectroscopic applications, and to a more sizeable geometry for the high-end spectroscopic applications, which require a beam energy of ~100 keV. Last, the scaling of *I'* with the source parameters, $I' \propto B' / \Delta E$, highlights the benefits of the high brightness and low energy spread of the CFE source and to a lesser extent, those of the Schottky source.

Task 2. Simulate the optical properties of the magnetic beam separator.

The electron-optical properties of the magnetic prism array, which separates the incoming and outgoing beam, strongly impact the design of the entire monochromator as the array geometry is central to defining the image planes, including that at the knife-edge, as well as the dispersion at this location, which directly impacts the monochromation.

The optical properties of simple magnetic prisms differ considerably in the plane that cuts across the top and bottom magnetic plates (the vertical plane) and the plane that separate these two plates (the horizontal or mid-plane), giving rise to large astigmatism and distortion. For the monochromator, the magnetic prism needs to concurrently provide a deflection of 90° while behaving as a round lens overall in order to preserve the quality of the illuminating beam. This behavior can be achieved in a beam separator that is composed of a close-packed magnetic prism array [Kolarik, Degenhardt, Mankos[c]]. Figures 4a and b show an example of such an array consisting of a large, central square region with a uniform magnetic field that connects the top and bottom plates, surrounded by several smaller sectors with individual coils to locally modify the magnetic field. The strengths of these fringe fields are tuned to match the focus in the vertical plane with that achieved naturally by the curvature in the path in the mid-plane.

PRISM, a proven software package developed by MEBS, Ltd. was used to calculate the electron-optical properties of 90° prism array configurations. In this package, prism arrays comprising magnet regions held at different magnetic excitations and separated by gaps consisting of grooves can be evaluated. The two-dimensional fields in the prism are calculated by a conformal mapping technique known as the Schwartz-Christoffel transformation. The software computes the optical axis, the multipole field components along the optical axis, the first order (paraxial) trajectories, the locations of the image planes, and the dispersion and the primary (second rank) geometrical and chromatic aberrations in these planes.

Trajectories are also computed by direct ray-tracing via a Runge-Kutta solution of the equations of motion to assess the full spot size at the knife-edge plane resulting from the convolution of the magnified source size at the crossover with the primary and higher-order aberrations of the prism.

The optical effects of the magnetic field in each sector and in the transition between sectors can be represented by a convex or a concave lens with disparate properties in the horizontal and vertical planes. As illustrated in Figs. 4c and 4d, each 90° deflection is thus a complex optical assembly that needs to be carefully optimized. In the simulations, the geometry of the individual sectors, the total number of sectors, as well as the individual sector excitations were varied in order to achieve the maximum possible energy dispersion with a practical beam separator design.

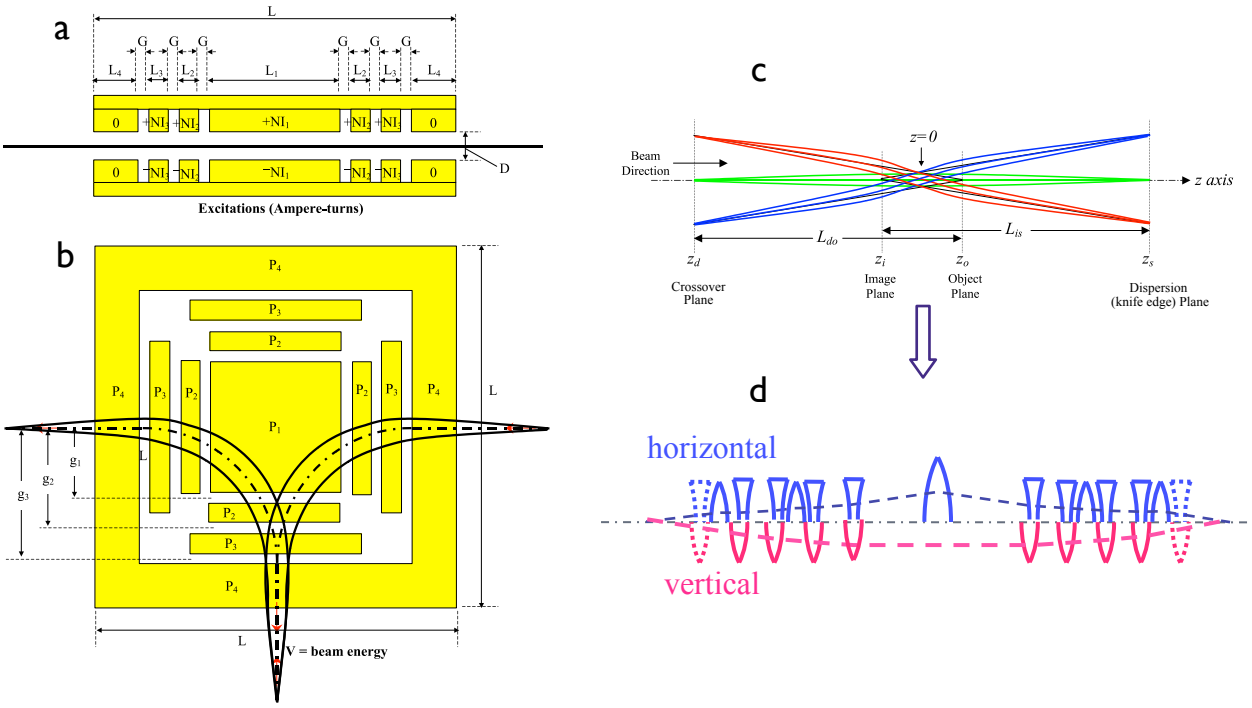

Figure 4. Magnetic prism array layout: a - cross-sectional view, b - mid-plane view, c - unfolded ray diagram along the curved beam axis, d - equivalent optical model along the unfolded axis.

The low voltage beam separator

The compact monochromator design for SEMs and TEMs operating at beam energies of 5-20 keV utilizes a magnetic prism array with an overall size of 100 mm x 100 mm, as shown in Fig. 5. This design produces a dispersion of 10.6 µm/eV at 5 keV and 2.6 µm/eV at 20 keV and can deliver a 10 meV resolution for the entire energy range by optimizing the values of the magnified source size and of the convergence angle at the crossover. The dispersion plane is located only 105 mm from the center, which makes for a short column, an important factor for minimizing Coulomb interactions. The performance of the beam separator at the beam energies of 5 keV and 20 keV is illustrated in Fig. 6. The figure shows a through-focus series of spot diagrams at the knife-edge as found by direct ray-tracing for two distinct electron beams that differ in energy by 10 meV. It should be noted that the largest contour in the spot diagrams

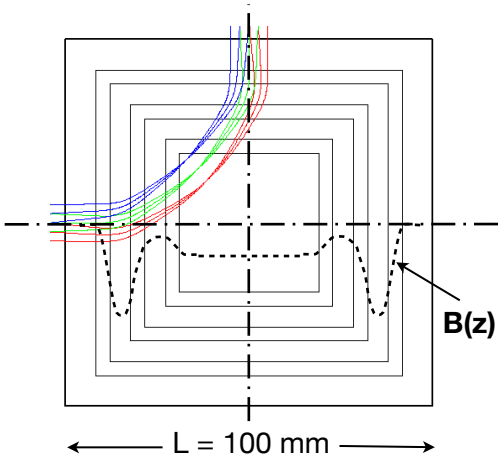

Figure 5. Layout of compact magnetic beam separator for 5-20 keV.

corresponds to 6σ, equal to the diameter that contains 99% of the current. Hence, 50% of the current is contained in a diameter that is approximately 40% of that of the largest contour.

The optimum values for the beam parameters at the crossover (magnified source size, convergence angle) for separating these two beams at 5 keV were found to be (75 nm, 0.8 mrad), providing 300 pA to the sample with a CFE source. At 20 keV, the optimum values were found to be (20 nm, 0.3 mrad), providing 2 pA to the sample with a CFE source. The current to the sample for the 5 keV would drop to a still practical value of 15 pA for a Schottky source.

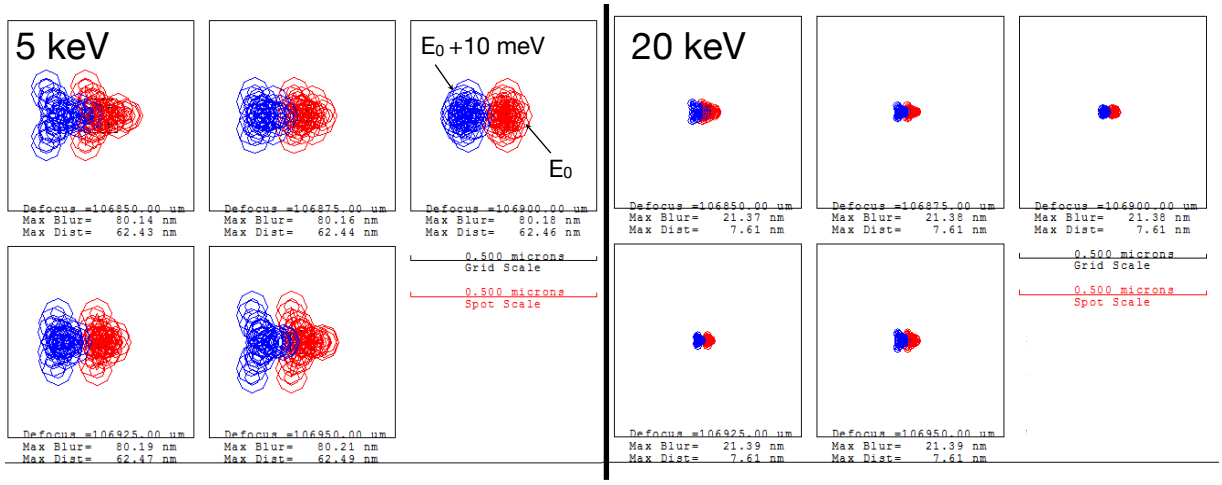

Figure 6. Through-focus series of beam blur in dispersion plane of compact beam separator for two electron beams with energy difference of 10 meV at 5 keV (left) and 20 keV (right).

The performance of this compact beam separator can be extended further at a 5 keV beam energy to give either better energy resolution or more sample current. The two cases are illustrated in Fig. 7. The energy resolution could be enhanced to 5 meV if the beam parameters at the crossover are chosen as (40 nm, 0.35 mrad). These values provide 3 pA to the sample with a CFE source. On the other hand, the current to the sample could be increased significantly for use cases where an energy resolution of 50 meV is sufficient, as it is for imaging applications with a low-voltage SEM. In this case, the crossover parameters can be increased to (400 nm, 1 mrad), delivering 3 nA to the sample with a Schottky source.

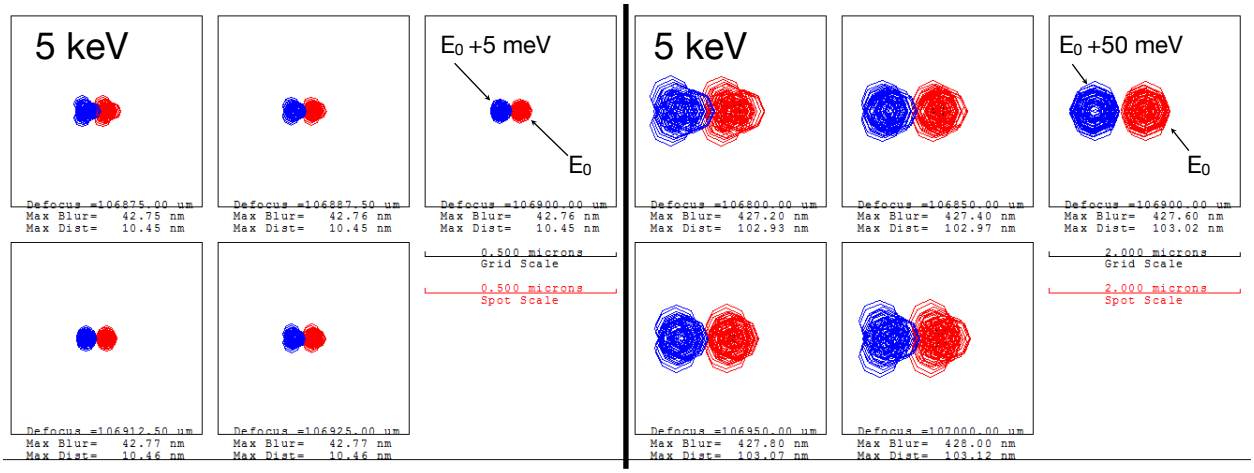

Figure 7. Through-focus series of beam blur in dispersion plane of compact beam separator for two electron beams with energy difference of 5 meV (left) and 50 meV (right) at 5 keV.

The high voltage beam separator

The monochromator design for TEMs operating at a beam energy of 100 keV utilizes a magnetic prism array with an overall size of 400 mm x 400 mm, as shown in Fig. 8 (left). It produces a dispersion of 2.7µm/eV and can deliver a 10 meV energy resolution. The dispersion plane is located 517 mm from the center, which still allows for a practical column design, as Coulomb interactions are significantly reduced at high beam energies. The performance of this beam separator is illustrated in Fig. 8 (right). The beam parameters at the crossover were optimized to the values (20 nm, 0.2 mrad), providing 15 pA to the sample with a CFE source.

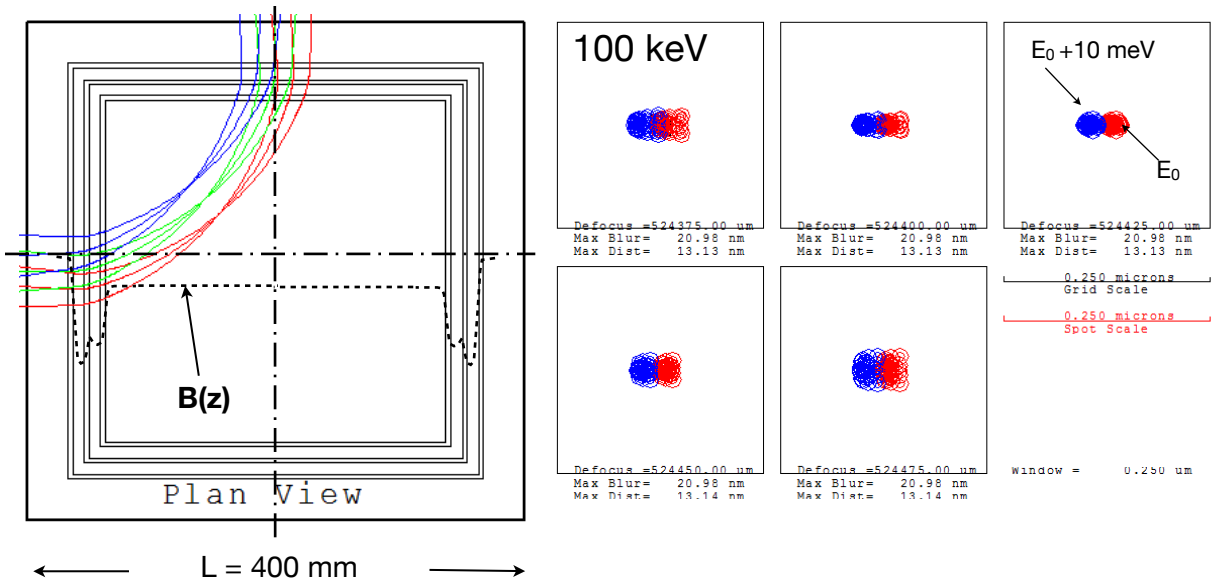

Figure 8. Layout of magnetic beam separator for 100 keV (left), and through-focus series of beam blur in its dispersion plane for two electron beams with energy difference of 10 meV.

The monochromator design can be adapted to the recently introduced TEMs operating at a lower beam energy of 20 keV [Kaiser]. First, the ultimate energy resolution can now be extended to as low as 3 meV, as illustrated in Fig. 9 (left). In this case, the crossover size at the entrance plane increases to 30 nm, and the convergence angle to 0.3 mrad to provide a sample current of 5 pA with a CFE source. While this current is relatively low, it is still suitable for high resolution imaging spectroscopy applications with an unprecedented 3 meV energy resolution. Second, the large energy dispersion will now support the use of a Schottky emitter for 10 meV resolution spectroscopy, as shown in Fig. 9 (right). In this case, the crossover size at the entrance plane can be increased to 100 nm, while the convergence angle can be made as large as 0.5 mrad to provide a sample current of 40 pA with a Schottky source. If a CFE emitter were to be used instead, the sample current would reach a whopping 1 nA, which would significantly reduce the spectrum acquisition times.

The key parameters of the above discussed beam separator modes are listed in Table 2. These modes include the effects of diffraction and the prism aberrations. They do not include the aberrations in the mirror and transfer lens optics nor the impact of Coulomb scattering. In the following sections, these remaining effects are investigated.

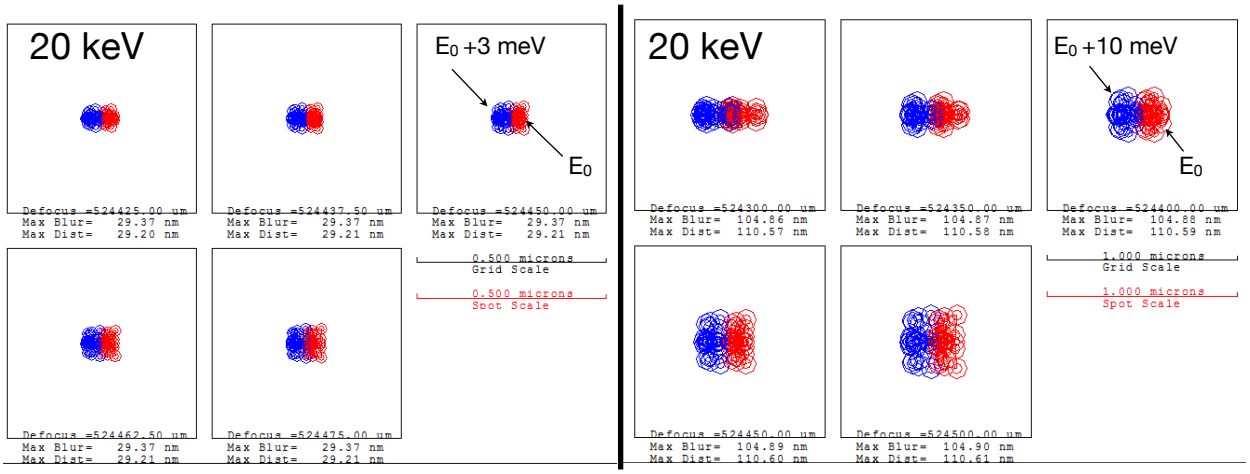

Figure 9. Through-focus series of blur in dispersion plane of the L=400mm beam separator for two electron beams with energy difference of 3 meV (left) and 10 meV (right) at 20 keV.

Beam energy [kV]	Prism length [mm]	Crossover size [nm]	Convergence angle [mrad]	Final beam current [pA]	Energy resolution [meV]
5 keV	100	40	0.35	$3^{(CFE)}$	5
5 keV	100	75	0.8	$15^{(Schottky)}$ $300^{(CFE)}$	10
5 keV	100	400	1.0	$3000^{(Schottky)}$	50
20 keV	400	30	0.3	$5^{(CFE)}$	3
20 keV	100	20	0.3	$2^{(CFE)}$	10
20 keV	400	100	0.5	$40^{(Schottky)}$ $1000^{(CFE)}$	10
100 keV	400	20	0.2	$15^{(CFE)}$	10

Table 2. Monochromator design options and their key optical parameters.

Task 3. Simulate the optical properties of the electron mirror.

The electron-optical properties of the electron mirror are key to introducing the symmetry in the electron path, which allows the use of the knife-edge aperture. After the 90° deflection in the beam separator, the beam is focused at the energy dispersion plane to achieve maximum energy resolution, after which it enters the electron mirror. The purpose of the electron mirror is to reflect the incoming beam and to refocus the beam at the dispersion plane.

The specialized software package MIRROR DA developed by MEBS, Ltd. was used for the analysis of the electron mirror optics. This differential algebra-based (DA) software package computes optical properties and aberrations of electron mirrors of any order and with any symmetry and can handle combinations of electron mirrors and electron lenses in a unified way. Results computed with MIRROR

DA were shown to be in good agreement with those extracted by direct ray tracing with relative deviations of less than 0.065% for all primary aberration coefficients [Munro].

A layout of the electron mirror optics and the distribution of the electrostatic potentials are shown in Fig. 10a. The electrons enter from the left and form a crossover in the dispersion plane, which is located a few

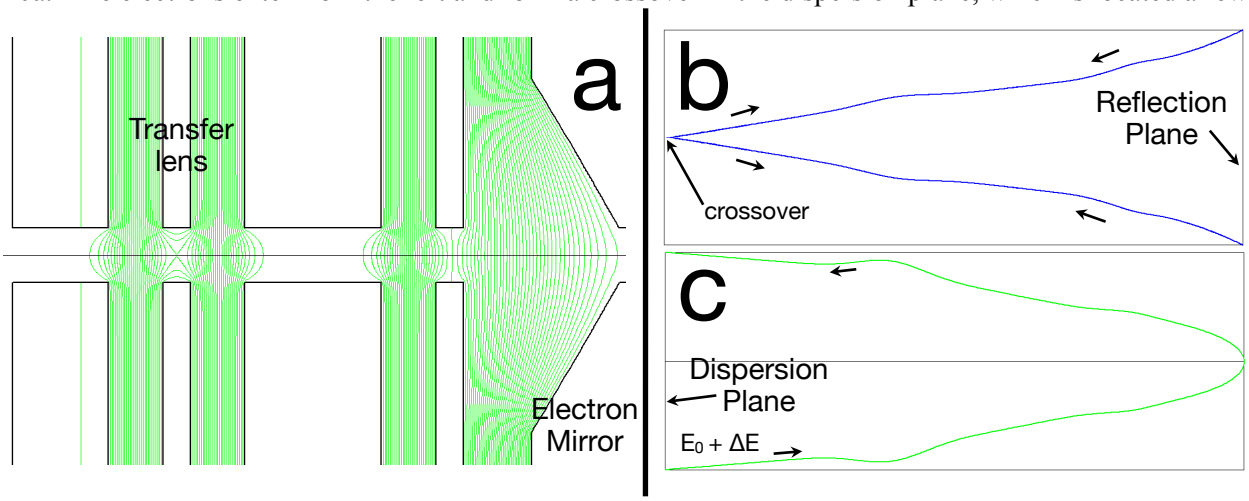

Figure 10. Layout of electron mirror (a); and axial (b) and field ray (c) in the electron mirror.

millimeters in front of the mirror optics. The beam crossover for the electrons with nominal energy E_0 is located on axis, while the crossover for electrons with higher energy $E_0 + \Delta E$ is displaced by a distance of $D \cdot \Delta E$, due to the prism dispersion D. The on-axis rays diverge when entering the mirror (Fig. 10b) and are reflected back onto themselves at the reflection surface. The beam divergence counters the rise in the current density from the vanishing electron speeds at this surface, thus minimizing the effect of Coulomb interactions in the mirror. The off-axis rays, those with higher energies $E_0 + \Delta E$, converge towards the center of the mirror (Fig. 10c) and are reflected by the mirror about the axis of symmetry, which directs them towards the knife-edge as desired.

As illustrated in Fig. 11, the aberrations of the mirror optics, comprising the transfer lens and the electron mirror, do not appreciably deteriorate the spatial resolution in the dispersion plane. As the geometric and chromatic aberrations increase with increased convergence angle, the cases with the largest convergence

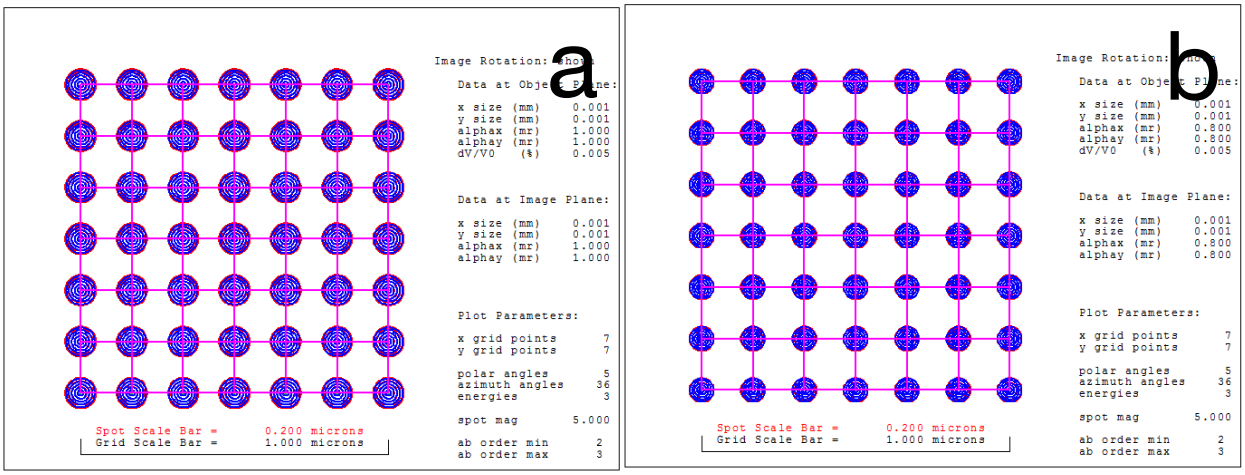

Figure 11. Blur diagram in dispersion plane for beam energy of 5 keV and convergence angle of 1 mrad (a) and 0.8 mrad (b).

angles outlined in Table 2 were considered first. Figures 11a and 11b show the blur in the dispersion plane after the electrons are reflected by the mirror for cases with a 5 keV beam energy. Figure 11a describes the case with a 1 mrad convergence angle, where the crossover spot size formed by the electrons in the dispersion plane prior to entering the mirror is 400 nm. Here, the total blur from all mirror aberrations is 19.8 nm, resulting in a negligible increase in the spot size to 400.5 nm. Figure 11b describes the case with a convergence angle of 0.8 mrad, where the spot size at the crossover upstream from the mirror is 75 nm. Here, the total blur from all mirror aberrations is 16 nm, resulting in a minor increase in the spot size to 76.7 nm.

Figures 12a and 12b show the blur in the dispersion plane after reflection for cases with a 20 keV beam energy. Figure 12a describes the case with a convergence angle of 0.3 mrad, where the spot size at the crossover upstream from the mirror is 20 nm. In this case, the total blur from all mirror aberrations is 1.5 nm, resulting in a negligible increase in the spot size to 20.1 nm. Figure 12b describes the case with a convergence angle of 0.5 mrad, where the spot size at the crossover upstream from the mirror is 100 nm. In this case, the total blur from the mirror aberrations is 2.4 nm, resulting again in a negligible increase in crossover size to 100.03 nm. For the case with a 100 keV beam energy (not shown), the added blur to the spot size of 20 nm is less than 1 nm.

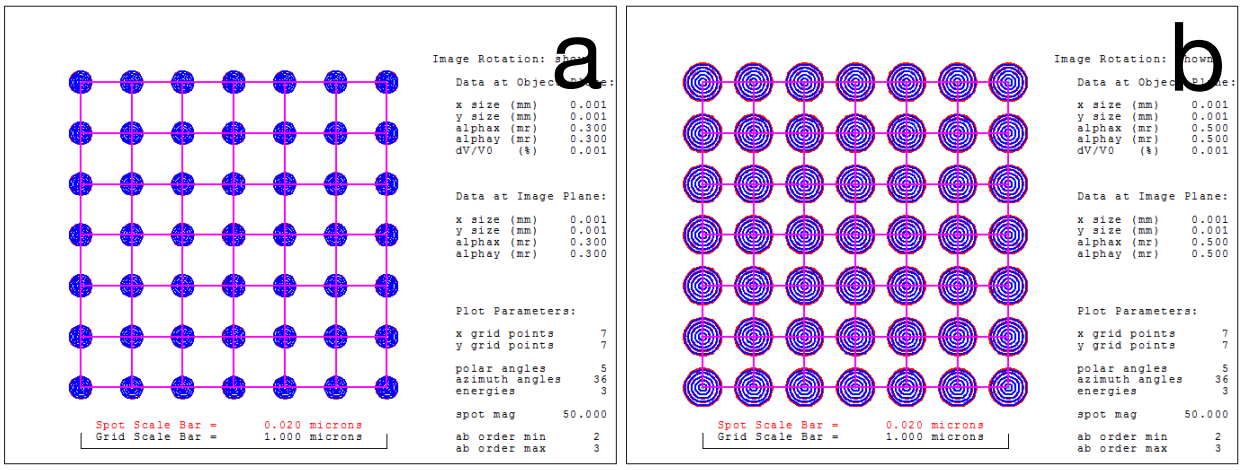

Figure 12. Blur diagram in dispersion plane for beam energy of 20 keV and convergence angle of 0.3 mrad(a) and 0.5 mrad (b).

Task 4. Simulate the electron-optical properties of the transfer lenses

The transfer lens system comprises round lenses that transport the beam from the electron source to the beam separator, from the separator to the electron mirror and back to the separator (as described in the previous section), and finally from the separator into the electron column. The lenses maintain the focus at the dispersion plane and assure proper ray symmetry and optimum magnification for high energy resolution. In the illumination optics, a minimum of two lenses is needed to maintain focus and to vary the magnification at the beam crossover. The optimum convergence angle is then selected by a set of round apertures with variable diameters.

Several specialized software packages, including the SOFEM and IMAGE, which are industry-standard packages developed by MEBS, Ltd. were used for the analysis of the transfer lens optics. SOFEM computes potential and field distributions in electrostatic and magnetic lenses and deflectors to very high accuracy using the second-order finite element method. The IMAGE software package computes effects of aberrations and discrete Coulomb interactions in electron beams in a unified way by direct ray-tracing. Accurate direct ray tracing eliminates the need of using conventional aberration theory making the method applicable to systems with aberrations of any order.

Both electrostatic and magnetic lenses were explored for the transfer lens systems. The geometry of the

individual lenses, as well their number and relative position were varied, and their first order optical properties were computed to achieve a practical lens design that meets the requirements on focus, magnification, and ray path symmetry.

The main contributors to the optical blur from the transfer lenses are due to their spherical (C_S) and chromatic (C_C) aberration coefficients. These aberrations add approximately in quadrature to the spot sizes shown in Table 2. The spot diameters associated with these aberrations are approximated as [Kruit]:

$$d_S = 0.18\ C_S\ \alpha^3 \qquad \text{(Spherical aberration)}$$

$$d_C = 0.34\ C_C\ \alpha\ \Delta E/E \qquad \text{(Chromatic aberration)}$$

The magnitudes of the spherical and chromatic aberration coefficients of electron lenses commonly used vary from 10 mm to 100 mm. For very short focal length lenses, they can approach 1 mm. Using the upper bound value of 100 mm for these coefficients, the blur due to spherical aberrations is approximated as 0.02 nm and is thus negligible. The blur due to chromatic aberrations for the 5 keV beam, where it has the greatest impact, is approximately 3.4 nm for the Schottky source and 1.4 nm for the CFE source, which also make negligible contributions to the spot sizes quoted in Table 2. Hence, as a result of the small convergence angles involved, the spherical and chromatic aberrations of the transfer lenses do not materially impact the optical performance of the monochromator.

Task 5. Model Coulomb interactions

Because the monochromator removes a significant fraction of the emitted electrons in order to reduce the energy spread, the starting currents, prior to monochromation, must be significant. Hence, the impact of Coulomb interactions in this region must be analyzed. Coulomb scattering can negatively impact the monochromator properties by increasing the beam energy spread (Boersch effect), which increases the chromatic aberrations, and by introducing trajectory displacement (Loeffler effect), which reduces the beam brightness. There is also the effect of the overall, average space charge, which defocuses the beam in the Gaussian plane and changes the image magnification [Jansen]. The defocus can be corrected for a uniform charge distribution in an axially symmetric beam by refocusing the lens [Mkrtchyan].

The IMAGE software package from MEBS Ltd. was used to evaluate the impact of Coulomb interactions. The software package computes electron-optical properties by propagating bunches of particles through realistic electromagnetic fields by accurate direct ray-tracing to capture the combined effect of Coulomb interactions and aberrations. The resulting energy spread and beam blur were calculated for a range of practical beam currents and electron energies. As the IMAGE code requires a straight axis, the magnetic beam separator is modeled as a rotation free magnetic lens doublet that images the crossover onto the dispersion (knife edge) plane with unit magnification and with a focal length given by the overall focusing strength of the beam separator along the unfolded axis (Figs. 4c, 4d). The simulation is divided into two steps: the first step simulates the Coulomb interactions from the electron source, through the beam separator, and onto the dispersion plane; the second step simulates the Coulomb interactions in the mirror, from the dispersion plane to the reflection surface and from this surface back to the dispersion plane. Here, the simulated current is reduced to half the beam current as the other half is removed by the knife edge.

The Coulomb blur increases with beam current *I* and system length *L* and decreases with beam energy [Jansen, Pfeiffer]. The blur scales approximately as $I^{5/6}\ L^{5/4} / \alpha^{3/5}\ r^{1/2}\ E^{3/2}$, where *r* is the beam radius. The largest impact of Coulomb interactions is thus expected for modes with a 5 keV beam energy, in particular for the case with 50 meV resolution, which benefits from the use of the highest primary current I, as high as 40 nA.

The increase in the spot size and in the energy spread at the dispersion plane from Coulomb interactions

during travel through the beam separator is illustrated in Fig. 13. The impact of Coulomb interactions in the mirror were found to be much less than that in the beam separator. The reason is that in the mirror, the path is shorter, the beam does not form an intermediate crossover, and the beam current is less by a factor of 2.

The FWHM of the crossover increases from 395 nm (no Coulomb interactions) to 457 nm with a beam current of 40 nA, and to 485 nm with a beam current of 40 nA. Coulomb interactions with the highest beam current in the mirror (20 nA) increase the blur by less than 10 nm, from 485 nm to 494 nm. The 25% overall increase in spot size is still small and will result in a tolerable loss of energy resolution to 65 meV. With a reduced primary beam current of 20 nA, the FWHM of the spot increases from 395 nm (no Coulomb interactions) to 457 nm. The path in the mirror with 10 nA of beam current increases the final spot size to 460 nm, yielding an energy resolution of 58 meV.

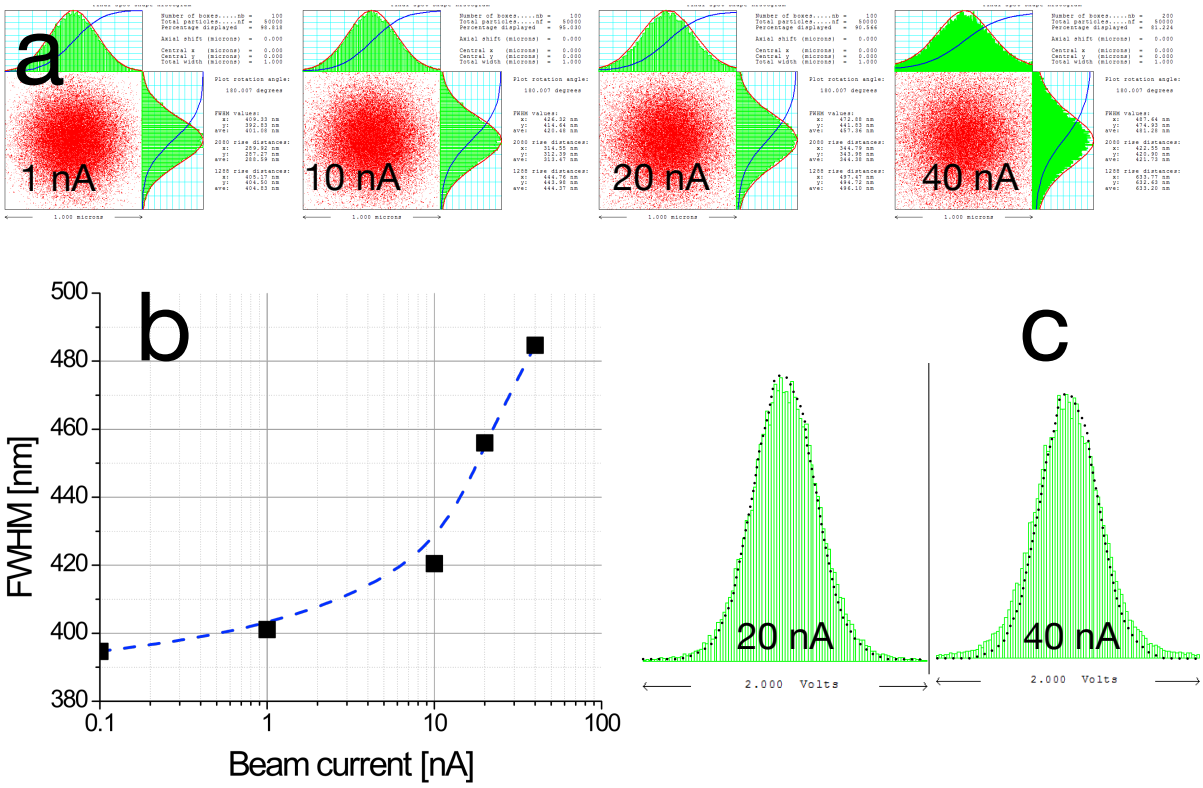

Figure 13. a and b - Beam spot in dispersion plane versus beam current at 5 keV beam energy, c - initial (dotted line) and final energy distribution at 20 and 40 nA beam current.

For the remaining modes at 5 keV, the impact of Coulomb interactions is even less noticeable. Simulations for the case with 10 meV resolution show that for the Schottky emitter with a 1 nA primary beam current, the impact is negligible, and for the CFE emitter with a 10 nA primary beam current, the spot size increases by ~ 10%, yielding a small loss of energy resolution to 11 meV. For the case with 5 meV resolution, the low primary beam current of 0.5 nA results in a negligible Coulomb contribution.

The impact of Coulomb interactions is further reduced at the higher beam energies. Out of the remaining modes, the only noticeable increase was found for the case with 10 meV resolution at the beam energy of 20 keV. This design utilizes the large beam separator (L = 400 mm) and a CFE capable of delivering a maximum primary beam current of 30 nA. In this case, the beam path through the prism is more than 4 times longer than for the 100 mm prism array, resulting in significant Coulomb interactions yielding an increase in the spot size from 100 nm to 151 nm. The contribution from the path in the mirror is significantly lower, as the length of the path in the mirror does not increase in proportion to the size of the

prism. In order to maintain the degradation in the energy resolution to a tolerable value of 10%-15%, the primary beam current must be reduced to 10 nA, yielding a still large sample current of 400 pA.

Task 6. Calculate the electron-optical parameters of the complete system

In the final step, the results obtained from simulating the optical properties of the beam separator, the electron mirror, the transfer lenses, and Coulomb interactions were folded into a complete model describing the key electron-optical parameters of the monochromator. Based on the findings, two optimum designs were derived: one for low voltage SEM and TEM applications (5-20 keV), and one for conventional TEM applications (up to 100 keV). A layout of the complete system with all the required system components is shown in Fig. 14.

Electrons emitted by the source are focused by the illumination optics to form a crossover upstream from the beam separator. The illumination optics consists of a gun lens, a condenser lens, and a variable round beam limiting aperture that sits between the two lenses. This system tunes the crossover position as well as the beam size and the convergence angle at this position in order to optimize the energy resolution that is obtained by the monochromator for a given application.

The beam separator, a magnetic prism array, deflects the beam off the microscope column axis by 90 degrees towards a module with a knife-edge that is backed by an electron mirror. The prism images the crossover at the location of the knife-edge, while dispersing the electrons in proportion to their energies. Electrons with lower or higher energies than the nominal value are cut off by the knife edge aperture before or after entering the mirror, respectively, thereby reducing the energy spread of the beam that is transmitted back into the beam separator. The transmitted beam is deflected once more by 90 degrees, refocused into a crossover, and transported into the optics of the electron microscope.

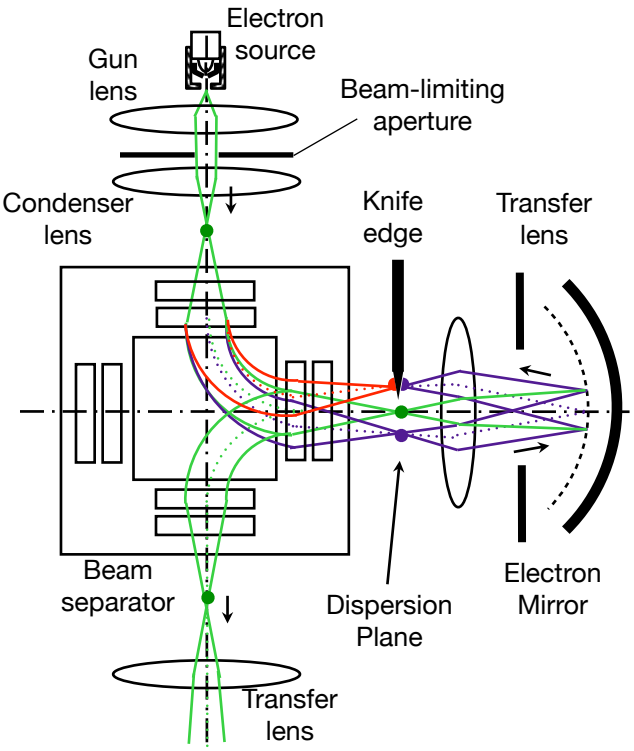

Figure 14. Monochromator system components.

The spot size at the knife-edge, which determines the degree to which a beam is monochromated, was calculated by taking into account the source brightness and initial energy spread, the diffraction from the beam limiting aperture, the aberrations from the lenses in the illumination optics, the prism, and the mirror optics, as well as the electron-electron Coulomb interactions.

The outcome of this analysis is the determination of practical operating modes for the monochromator and their key performance characteristics, as described by the energy resolution and the beam current that is transmitted to the sample. The dependence of the transmitted current on the energy resolution and on the beam energy favors the bifurcation of the application space into two distinct cases: one for high speed imaging applications that work with a moderate energy resolution and one for high-end spectroscopic applications that sacrifice sample current for energy resolution. The former employs a compact, 100 mm prism array, while the later uses a larger, 400 mm array. For either application, a Schottky or CFE emitter can be used. A summary of key parameters for these two monochromator options are listed in Table 3.

LVSEM: 100 mm separator

Beam energy [kV]	Energy resolution [meV]	Max. beam current Schottky emitter [pA]	Max. beam current Cold field emitter [pA]
5 keV	5	n/a	3
5 keV	10	15	300
5 keV	50-65	3000	3000
20 keV	10	n/a	2

TEM: 400 mm separator

Beam energy [kV]	Energy resolution [meV]	Max. beam current Schottky emitter [pA]	Max. beam current Cold field emitter [pA]
20 keV	3	n/a	5
20 keV	10	40	1000
100 keV	10	n/a	15

Table 3. Key optical parameters of monochromator for the Low voltage SEM and spectroscopic TEM design options.

III. Significance of Phase I Results.

In Phase I, we successfully demonstrated that the proposed mirror monochromator can reduce the energy spread of high brightness electron sources to 10 meV for practical values of the beam current and that further reduction of the energy spread to 3 meV is possible. Detailed electron-optical analysis of the monochromator system and its key components was performed using state-of-the-art simulation software, yielding an optical design that is suitable for a monochromator prototype. We have completed all the tasks and have met the milestones outlined for Phase I. The key risks have been retired, and Electron Optica is now ready to embark on building the prototype in Phase II.

IV. Bibliography & References Cited

Degenhardt, R., Korrektur von Aberrationen in der Teilchenoptik mit Hilfe von Symmetrien, Ph.D.Dissertation (1992), Technische Hochschule Darmstadt.

Jansen, G.H., J. Appl. Phys. 84 (1998), p. 4549.

Kaiser, U., et al., Transmission electron microscopy at 20 kV for imaging and spectroscopy, Ultramicroscopy 111 (2011), p. 1239–1246.

Kolarik, V., Venklasen, L.H., Mankos, M., Close packed prism arrays for electron microscopy, Optik 87 (1991), p. 1-12.

Kruit, P., Bezuijen, M. and Barth, J. E., Source brightness and useful beam current of carbon nanotubes and other very small emitters, J. Appl. Phys. 99 (2006), p. 024315.

Mankos[a], M., Mirror monochromator for charged particle beam apparatus, U.S. Patent # 8,183,526, May 22, 2012.

Mankos[b], M., Adler, D., Veneklasen L., Munro, E. , Electron optics for high throughput low energy electron microscopy, Surface Science 601 (2007), p. 4733-41.

Mankos[c], M., Spasov, V., and Munro, E., Principles of Dual-Beam Low-Energy Electron Microscopy. In Peter W. Hawkes, editor: Advances in Imaging and Electron Physics, Vol. 161, Burlington: Academic Press, (2010), pp. 1-53.

Mkrtchyan, M.M., Liddle, J.A., Berger, S.D., Harriott, L.R., J. Appl. Phys. 78, (1995), p. 6888.

Pfeiffer, H., New prospects for electron beams as tools for semiconductor lithography, Scanning Microscopy 2009, edited by Michael T. Postek, Dale E. Newbury, S. Frank Platek, David C. Joy, Proc. of SPIE Vol. 7378 (2009), p. 737802. doi: 10.1117/12.822771